Compaction and cementation control on bleaching in Triassic fluvial red beds, S-Germany

Christina Schmidt, Benjamin Busch & Christoph Hilgers*

Schmidt, C., Busch, B. & Hilgers, C. (2020): Compaction and cementation control on bleaching in Triassic fluvial red beds, S Germany. Z. Dt. Ges. Geowiss.

Abstract: This study focusses on bleaching phenomena on the pore scale in an Olenekian (Upper Buntsandstein) sandstone quarry. The study area exposes a 10 m thick red sandstone body with up to cm sized, greyish white laminae in sandstones. Analyses focus on bleached and unbleached zones in the same cm sized samples.

Bleached zones show a larger grain size (by 27 µm), less compaction and a higher porosity (by 3 %). They also exhibit stronger cementation by all observed authigenic phases of quartz, illite, K feldspar and to a minor extent dolomite. Calcu lated intergranular volumes and cementational porosity loss also correlate positively with bleaching. Meanwhile unbleached zones contain more ductile grains (e.g. micas, detrital clay, rock fragments like phyllites and plutonic rock fragments) and are affected by major porosity loss via compaction.

Bleaching is related to primary features like grain size selective lamination and associated higher permeability in coarse grained laminae. It is also reliant onto an early framework stabilising cement phase, which keeps pathways open for uplift related leaching of the detritus and few dolomite cements.

Kurzfassung: Die folgende Studie betrachtet Bleichungsphänomene auf dem Porenmaßstab in einem Sandsteinbruch des Olenekiums (Oberer Buntsandstein). Das Untersuchungsgebiet umfasst einen 10 m mächtigen, roten Sandsteinkörper, wel cher bis zu cm mächtige, gräulich weiße Laminen enthält. Fokus der durchgeführten Analysen sind gebleichte und unge bleichte Zonen in einzelnen cm großen Proben.

Gebleichte Zonen besitzen eine größere mittlere Korngröße (um 27 µm), zeigen eine weniger ausgeprägte Kompaktion und eine höhere Porosität (um 3 %). Quarz, Illit, K Feldspat und in geringem Maße Dolomit treten als authigene Zement phasen in diesen Bereichen vermehrt auf. Berechnete intergranulare Volumina und die Porositätsverluste durch Zementation zeigen ebenfalls eine positive Korrelation mit gebleichten Bereichen. Derweil enthalten ungebleichte Zonen mehr duktile Klasten (z. B. Glimmer, detritischen Ton, Lithoklasten wie Phyllite und plutonische Gesteinsfragmente) und sind vor allem von Porositätsverlusten durch Kompaktion betroffen.

Die Bleichung ist verbunden mit primären Gesteinseigenschaften wie korngrößenselektiv Lamination und einer damit verbundenen höheren Permeabilität in grobkörnigeren Laminen. Zugleich ist die Bleichung abhängig von einer frühen, das Korngefüge stabilisierenden Zementphase, welche Fließwege offen hält für eine Alteration des detritischen Mineralbestands und der wenigen Dolomitzemente während der finalen Hebung der Formation.

Keywords: diagenesis, bleaching, reservoir quality, Triassic red beds

Schlüsselwörter: Diagenese, Bleichung, Reservoirqualität, triassische Sandsteine

1. Introduction

Various authors have described bleaching (discolouring) in continental red beds, reflected by the disappearance of the sediment's original red colour. Bleached specimens have been described from Lower and Middle Permian (Gaupp et al. 1993; Hilse et al. 2010; Pudlo et al. 2012; Schöner & Gaupp 2005), Lower Triassic rocks in Central Europe (Beyer et al. 2011, 2014; Hilse et al. 2010; Kasch et al. 2010; Kunkel et al. 2018; Wendler et al. 2012), Jurassic rocks in Utah and Nevada, USA (Beitler et al. 2003; Chan et al. 2000; Eichhubl et al. 2004; Parry et al. 2004) and elsewhere. Such phenomena may be pervasive or lamina-bound bleaching, or may have a speckled appearance or halos around clay clasts (Beitler et al. 2003; Beyer 2015; Chan et al. 2000; Hilse et al. 2010; Pudlo et al. 2012; Schöner & Gaupp 2005). Tectonic structures like joints, faults and deformation bands may also be associated with bleached lithologies (Busch et al. 2017; Eichhubl et al. 2004; Kasch et al. 2010; Parry et al. 2004; Wendler et al. 2012). The sediment's red colour originates

*Address of the authors:
Karlsruhe Institute of Technology, Structural Geology and Tectonics, Adenauerring 20a, 76131 Karlsruhe, Germany (christina.schmidt2@kit.edu)

from red pigments forming pigmented dust rims or continuous coatings around detrital grains. The red colour forms via the alteration of iron-bearing grains and infiltrated iron-bearing clay under oxidising Eh-conditions and neutral to alkaline pH in situ and after the settling of the sediment, respectively (Amelung et al. 2018; Walker 1967a, b; Walker et al. 1978; Weibel 1998).

The process of bleaching may be a process initiated by the migration of fluids causing a reducing environment at low pH and elevated salinities (Chan et al. 2000; Parry et al. 2004; Schöner & Gaupp 2005; Weibel 1998). Potential reducing and thus bleaching agents are hydrocarbons, methane, organic acids and hydrogen sulphide, which lower the redox potential of the fluid that subsequently reduces the hematite of the formation. Depending on the reactants, CO_2, water and sometimes pyrite are produced (Chan et al. 2000; Eichhubl et al. 2004; Garden et al. 2001; Gaupp et al. 1993; Gaupp & Schöner 2008; Haszeldine et al. 2005; Parry et al. 2004; Schöner & Gaupp 2005; Shebl & Surdam 1996; Weibel 1998). The reduction of hematite leads to an increase in mobile Fe^{2+} in solution that is then available for local removal. At higher Eh of the pore fluid, a proximal, subsequent oxidation to Fe^{3+} and re-precipitation as iron (and manganese) oxide concretions is possible (Chan et al. 2000; Parry et al. 2004). A reduction of hematite can also be triggered by microbial activity with the organisms' enzymes reducing the metal species (Dong et al. 2014; Lovley et al. 1993). Alternatively, bacteria can reduce sulphate consuming organic matter and forming e.g. H_2S, which in turn reduces hematite (Kirkland et al. 1995; Machel 2001; Schumacher 1996). Bacterial sulphate reduction is commonly replaced by thermochemical sulphate reduction at higher subsurface temperatures but also consumes organic matter (Machel 2001). Similarly pedogenesis may lead to colour mottling where e.g. stagnant groundwater locally constituted a reducing micro-environment (Amelung et al. 2018; Buurman 1980; Molenaar 1984). Wendler et al. (2012) also associate CO_2-rich fluids with bleaching and deduce a volcanic or meteoric origin. CO_2 influxes may cause a pH-decrease contributing to iron mobilisation (Schöner & Gaupp 2005).

Pudlo et al. (2012) describe bleaching on a regional scale to be restricted to specific depositional settings like fluvial channel fills and aeolian dunes rather than sandflat or even lacustrine deposits, while Beyer (2015) observes bleaching principally in e.g. sandflat deposits. Beyer (2015) relates bleaching to factors like grain size and cement content promoting fluid-rock interactions. For the Lower Triassic in Central Germany bleaching was associated with medium-grained sandstones with early blocky cements, mostly carbonates and sulphates, which occur mostly in cross-bedded sandstones and can be interpreted as sand sheet or channel fill facies (Kunkel et al. 2018). Schöner & Gaupp (2005) deduce from bitumen staining that bleaching is not facies-bound but merely correlates with bitumen impregnation or as proposed by Beyer (2015) with acidic fluids preceding hydrocarbon emplacement. However, no consistent model can be established. While some studies show that bleaching, petrophysical properties, and lithofacies are related (Beyer 2015; Eichhubl et al. 2004; Pudlo et al. 2012; Reinecker et al. 2015), other data neither suggest a correlatable impact of those properties on bleaching nor do they deny it (Beyer 2015; Kunkel et al. 2018; Schöner & Gaupp 2005).

In this study, we present data on a Lower Triassic red bed deposit with different amounts of decolouring, which is attributed to bleaching. We discuss lamina-bound and speckled decolouring with respect to sandstone petrology attempting at a better understanding of textural characteristics influencing the bleaching mechanism and evaluate its effect on reservoir properties.

2. Geological Setting

The study area Röttbach is located 5 km N of the town Wertheim, Central Germany, and is part of the German Triassic (Hagdorn et al. 2009; Meschede & Warr 2019; Okrusch et al. 2011). According to the regional stratigraphy, the Lower Triassic deposits in the Röttbach quarry belong to the Plattensandstein (Röt Formation) of the late Olenekian (Upper Buntsandstein; Menning 2018; Okrusch et al. 2011; Röhling et al. 2018). They were deposited as marginal facies at the southern border of the North German Basin (Freudenberger et al. 2013; Hagdorn et al. 2009; Okrusch et al. 2011; Ziegler 1990). Source areas are primarily the Vindelician High of Southern Germany and Switzerland to the SE and to a minor extent the Ardennes and Gallic Massif of France and Belgium to the W (Freudenberger et al. 2013; Hagdorn et al. 2009; Meschede & Warr 2019; Röhling & Lepper 2013; Ziegler 1982; Fig. 1). Correlations of Buntsandstein sequences across the marginal facies of Southern Germany are detailed in Röhling et al. (2018: Fig. 5).

The Lower Triassic sandstones evolved from braided geometries in the Induan and early Olenekian (Early and Middle Buntsandstein), towards occasionally ephemeral, meandering streams during the late Olenekian to Anisian (Upper Buntsandstein; Okrusch et al. 2011; Freudenberger et al. 2013). Those meanders are described to have a relatively constant position, low incision depth but may meander over a large width (Freudenberger et al. 2013; Okrusch et al. 2011). The late Olenekian Lower Röt claystones have been deposited in a sabkha to playa environment (Okrusch et al. 2011). They consist of silt- and claystones and can contain salt or sulphate nodules (Freudenberger 2016; Mader & Teyssen 1985; Okrusch et al. 2011).

The Plattensandstein, the focus of this study, has a thickness of up to 34 m in the study area (Freudenberger et al. 2013). Triassic Olenekian rocks are overlain by Anisian sediments, and locally crosscut by Upper Cretaceous to Tertiary basaltic and phonolitic volcanic dykes in the study area (Okrusch et al. 2011). The nearest reported exposure is a Tertiary explosive tuff chimney of 200 × 150 m diameter situated 31 km WNW of the study area (Okrusch et al. 2011).

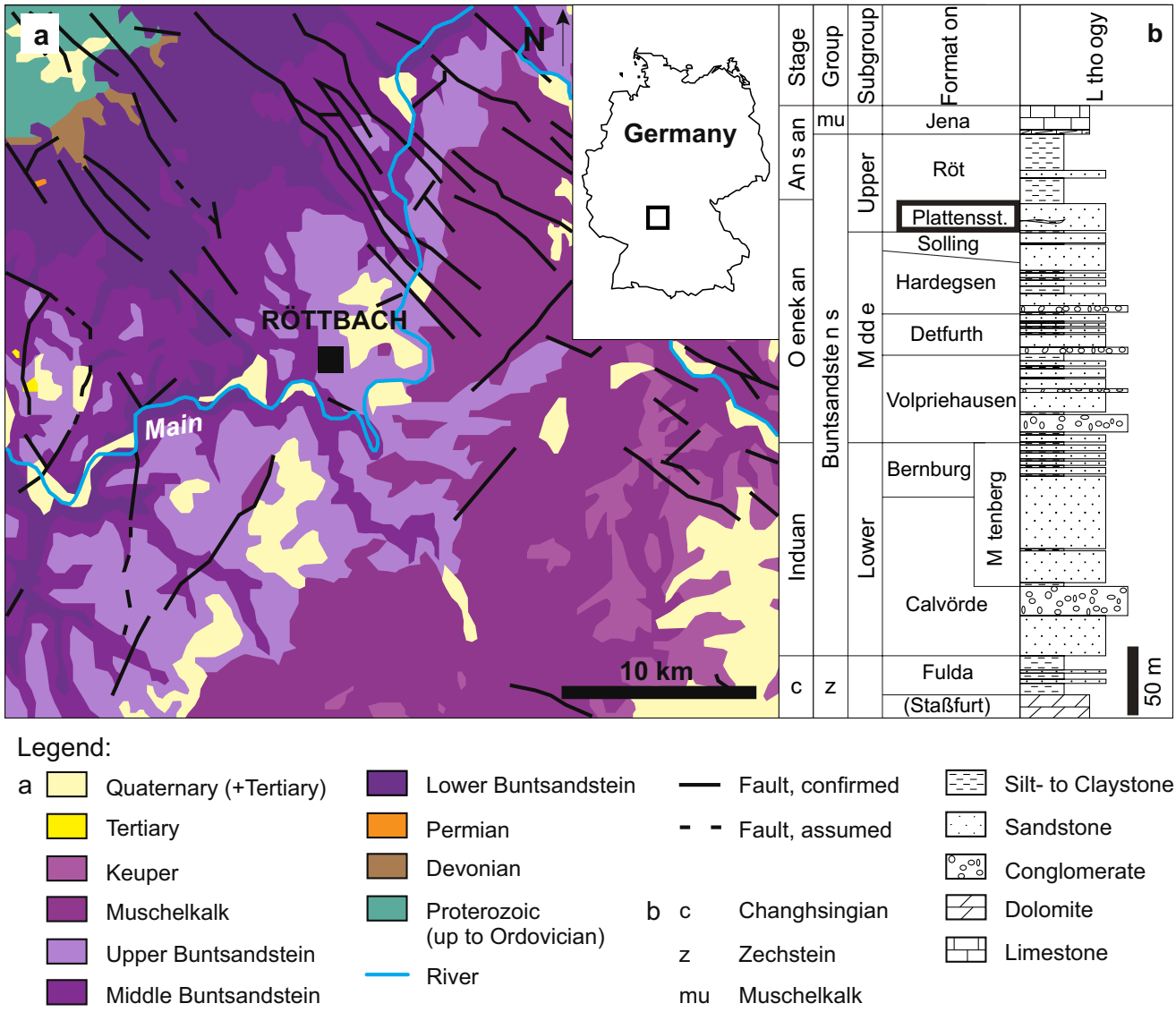

Fig. 1: (**a**) Location of the study area on the geological map of the SE margin of the Spessart (after Okrusch et al. 2011). (**b**) Lithological column displaying the stratigraphic position of the Plattensandstein, late Olenekian, (black box) in the footwall of the Lower Röt Claystone Member, Röt Formation (Upper Buntsandstein Subgroup); after Okrusch et al. (2011), modified from Geyer (2002).

3. Materials and methods

3.1 Sampling

The sandstone samples were drilled from the quarry wall (N = 36) as well as from mined m-sized blocks with distinctive bedding (N = 7). The 43 one-inch plugs were cut to lengths between 2.5 and 4 cm and oven-dried at 40 °C for seven days. Thin sections were prepared from resulting plug caps. Of those 43 samples, only eleven exhibit bleaching phenomena, two of them are fully bleached (RB-06, RB-07; Fig. 2, Supplementary Table). The nine partially bleached samples, containing lamina-bound and speckled bleaching, were used to compare the characteristics of the unbleached and bleached material within one sample (RB-04, RB-05, RB-17, RB-24, RB-26, RB-28, RB-35, RB-38, RB-42). All other samples were completely unbleached and are used as a reference for unbleached zones in samples with bleaching.

3.2 Petrography and porosity

Plug caps were impregnated with blue-dyed epoxy and thin sections prepared from them with a thickness of 30 µm, nine samples were stained with a combination of Alizarin Red S and potassium ferricyanide to identify carbonate cements.

Grain size was measured separately for both unbleached and bleached zones. Grain size analysis is done on a Leica

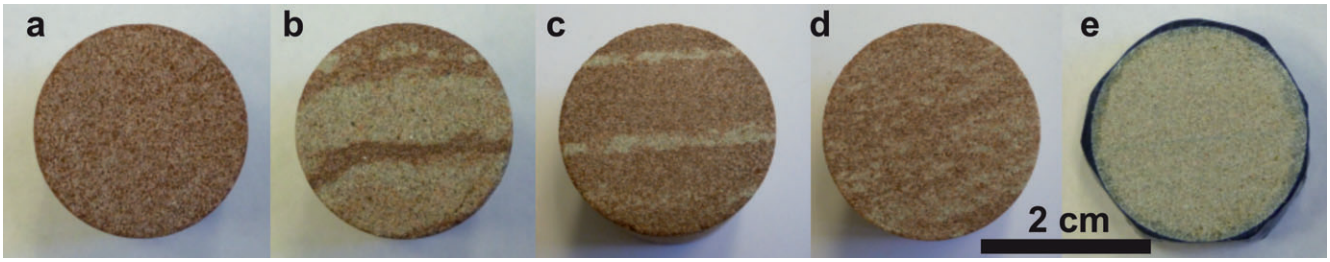

Fig. 2: Examples for different grades of bleaching in plugs. Partial bleaching occurred primarily lamina bound. Displayed is the range from unbleached brownish red (**a**: sample RB 30) to partially bleached, yellowish to greyish white samples (**b**: sample RB 28, **c**: sample RB 38, **d**: sample RB 42) and fully bleached yellowish white samples (**e**: sample RB 06).

DMLP microscope determining the length of the long axes of 100 detrital grains per thin section on a grid adjusted to the largest grain size to gain area-weighted results of the apparent grain size in 2D (Becker et al. 2017; Busch et al. 2020, 2019, 2017; Walderhaug 2000; Walderhaug et al. 2012; Wüstefeld et al. 2017). Dust rims of hematite pigments trace the original detrital grains and are used to distinguish them from authigenic cement and assess the detrital grain size (Busch et al. 2017). Subsequently, the grain size class was determined according to the Udden-Wentworth scale (Udden 1914; Wentworth 1922) and the degree of sorting was calculated using the formula by Folk & Ward (1957). The bias of the measurement introduced when measuring on 2D sections is approximated in two samples (RB-10, RB-28) when measuring the grain's long axis with or without the dust rim on 20 grains. Measuring the dust rim as part of the grain resulted in an average grain size larger by 6 to 8 µm. Grain morphology for both bleached and unbleached zones was assessed using the comparator after Füchtbauer (1988).

Point counting was performed on a Leitz Aristomet transmitted light microscope, fitted with a semi-automatic Pelcon Point counting stage and the grid adjusted to the maximum grain size. The specific modal composition was analysed separately for both unbleached and bleached zones (300 steps for each zone) in the nine samples exhibiting partial bleaching. Uniformly coloured thin sections and both unbleached and bleached zones in partly discoloured thin sections were point counted with 300 steps.

Each lithoclast or rip-up clast was counted once and their internal components were not considered during point counting. Two samples contained rip-up clasts of several mm in diameter (RB-17, RB-19). Those were neglected during point counting of the bulk thin section but RB-17 was included in the selective point counts of the unbleached and bleached zone. Iron oxide phases (pore-lining and filling) are point counted as a detrital phase, since their ductile deformation due to compaction makes a clear distinction of authigenic and detrital iron oxide phases difficult. Dust rims were used for the distinction between authigenic and detrital phases of quartz (Busch et al. 2017). Comparison of cement volumes deduced from transparent thin section and cathodoluminescence analysis shows that cement volumes can accurately be assessed by transmitted light microscopy (Makowitz & Sibley 2001; Walderhaug 2000). Results for the detrital composition are plotted in a QFR-plot according to Folk (1980) with normalised amounts of detrital quartz (Q), feldspar (F) and rock fragments (R).

The porosity was determined separately for both unbleached and bleached zones in the partially bleached samples by point counting. Microporosity was calculated from point counts based on mean fractions of microporosities in kaolinite, chlorite and illite after Hurst & Nadeau (1995) and the average of those values for undifferentiated clay minerals. The sum of the calculated microporosity and point counted primary and dissolution pore space constitutes the total point counted porosity.

The type of grain-grain contacts and the reduction of initial porosity can quantify compaction. Grain contact description follows the classification of Taylor (1950) as tangential or point (P-), long (L-), concavo-convex (C-) and sutured (S-) contacts and is applied to bleached and unbleached zones, reflecting increasing compaction (Taylor 1950). Accordingly, grains in loosely compacted sediments without contacts are named floating grains (F-contacts). To quantitatively derive the degree of compaction those five categories have been point counted among 100 grains in both unbleached and bleached zones. For each grain the contact was counted, which exhibited the strongest indication for compaction. Additionally, the contact strength was calculated for grain-to-grain contacts as a measure of compaction with higher values representing a higher degree of compaction (Füchtbauer 1967). Intergranular volume (IGV) is calculated from point counting data according to Paxton et al. (2002). The IGV is the sum of the intergranular pore space, intergranular cement volumes and depositional matrix, it is indicative of the degree of compaction (Paxton et al. 2002). Subsequently, further parameters can be determined based on the intergranular volume or minus-cement porosity as defined by Lundegard (1992), which is optical porosity plus intergranular cement volume. This includes porosity loss due to compaction (COPL) and porosity loss due to cementation (CEPL; Lundegard, 1992). The initial porosity is assumed to be 45 % according to Wilson & McBride (1988) for unconsolidated sand in a fluvial environment. Porosity loss by compaction is plotted against cementational porosity loss (Lundegard 1992).

4. Results

Bleached versus unaltered material

Macroscopic description, texture and structure

Bleaching is primarily lamina-bound but not strictly limited to a single lamina (see Figs. 2b, c). Such bleached laminae are up to 1 cm thick and extend over ≥1 m. Of the eleven bleached samples, two are completely bleached (e.g. Fig. 2e), two exhibit bleached laminae of various thickness (up to 8 mm thick; Fig. 2b, approx. 1 mm thick in Fig. 2c). The remaining seven display speckled but still bedding-parallel bleaching up to 3 mm in diameter (Fig. 2d). The weathered outcrop walls barely show bleaching; bleaching was visible in mined blocks and after sampling. No indication of a specific propagation direction of the decolouration apart from along laminae is given. Precipitation of iron phases either by abiotic components (Liesegang) or by biotic components (iron-oxide cement bands; Burgess et al. 2016) was not encountered.

For the eleven samples exhibiting bleaching, the average grain size of bleached zones is 173 µm (max. 185 µm, min. 151 µm), while the respective unbleached zones in the same samples have an average grain size of 146 µm (max. 163 µm, min. 130 µm; Fig. 3a). In each of those samples a discrepancy of 16 to 40 µm between the average grain size of the bleached and unbleached zone is found (Fig. 3b). The fully bleached samples both have average grain sizes of 176 and 182 µm (sample RB-06 and RB-07; Supplementary Table).

In samples with bleached laminae, all unbleached zones are moderately sorted. For the bleached zones and fully bleached samples, four of eleven samples are well sorted. The grains' roundness does not show any distinctive changes between unbleached and bleached zones. Both contain subangular to subrounded grains (Figs. 6a, b, Supplementary Table).

Petrography

Quartz grains constitute equally high fractions of the overall mineral assemblage in both unbleached (avg. 35 %, max. 43 %, min. 27 %) and bleached zones (avg. 38 %, max. 46 %, min. 28 %) (Fig. 4). Detrital K-feldspar grains account for on average 8 % (max. 11 %, min. 4 %) in unbleached zones and for 11 % (max. 16 %, min. 7 %) in bleached zones. Rock fragments are present with 7 % (max. 11 %, min. 4 %) in unbleached zones. In bleached zones they make up 7 % (max. 11 %, min. 4 %) of the rock.

Generally, bleached zones are characterised by more blue-dyed intergranular pore space than is visible in unbleached areas (Figs. 5a, b). Intragranular macropores larger than the average grain size occur only in bleached zones (Fig. 5c). They are identified by their remaining dust rim (Fig. 5c), illite fibres surrounding the resulting pore space, and meshwork illite partially filling such intragranular macropores (Figs. 5f, h). Both, unbleached and bleached zones, are affected by intragranular dissolution with on average 0.4 % (max. 1 %, min. 0 %) and 1 % (max. 4 %, min. 0 %), respectively (Fig. 6c).

Grain contacts are primarily concavo-convex contacts in unbleached zones (Figs. 5b, d, 6). On average 56.9 % of concavo-convex, 3.7 % sutured, 37.5 % long contacts are counted and the remaining 1.9 % are point contacts and floating grains (Supplementary Table). A different trend is observed in bleached zones: Only 23.1 % of the contacts are concavo-convex, 0.3 % sutured, 47.3 % long and 24.2 % point contacts as well as 5.1% floating grains (Supplementary Table). In all unbleached zones more than half of the grain contacts are contributed by concavo-convex and sutured contacts (51 % to 77 %), while in bleached zones concavo-convex and sutured contacts make up 15 to 33 % (Fig. 6). The contact strength after (Füchtbauer 1967) ranges for unbleached zones from 2.5 to 2.8 with an average value of

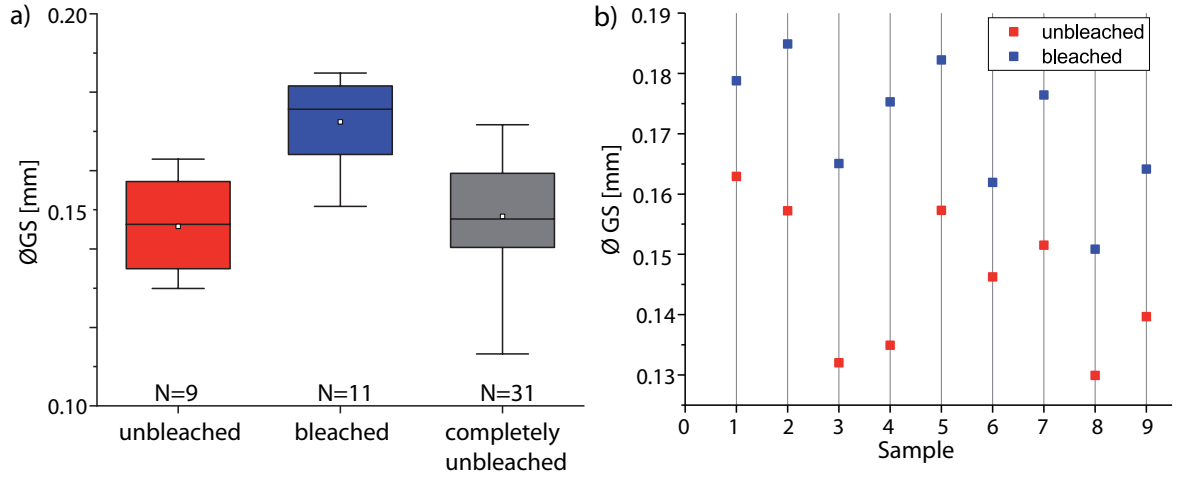

Fig. 3: (**a**) Box whisker plot of average grain sizes (ØGS) plotted for the three types of material: red unbleached zones, white bleached zones and completely red thin section samples (grey). The mean average grain size of bleached zones (avg. 173 µm) exceeds the un bleached zones (avg. 146 µm) by 27 µm. Completely unbleached samples cover the grain size range of all unbleached zones and reach a maximum grain size similar to the mean average grain size of the bleached zones. (**b**) The scatter plot for the nine partially bleached, indi vidual samples shows that bleaching in each sample coincides with a constantly larger average grain size.

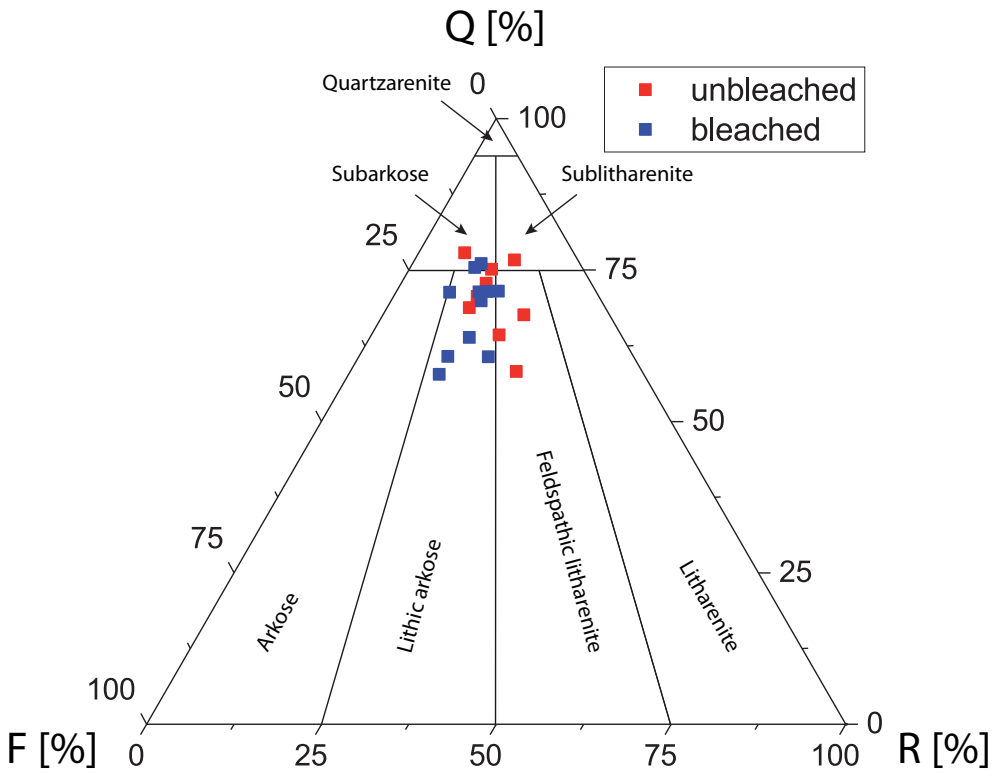

Fig. 4: QFR plot after Folk (1980) displaying the detrital composition including quartz (Q), feldspar (F) and rock fragments (R) of the samples for unbleached zones (red, N 9) and bleached zones (blue, N 11). Quartz is present in almost equal amounts in both sample types.

2.6. Bleached zones exhibit contact strengths from 1.9 to 2.2 with an average of 2.0 (Supplementary Table).

Iron oxides are present with on average 17.3 % in unbleached zones, bleached zones yield on average 0.5 %. A qualitative assessment shows that iron oxides are present in bleached zones constituting dust rims as pigmentation along the grain outline and underneath authigenic cements (Figs. 5a, c).

Quartz cements constitute 12 % in unbleached and 18 % in bleached parts (Figs. 5c, f, g, h, 7a, b). Similarly, the illite content in bleached zones (avg. 11 %) exceeds that in unbleached ones (avg. 8 %; Figs. 5c, f, 7a, c). K-feldspar cement represents 7 % in the bleached zones whereas unbleached zones contain on average 4 % of K-feldspar cement (Figs. 5c, f, g, h, 7a, d). Other authigenic phases are dolomite (unbleached: avg. 0.1 %, bleached: avg. 0.5 %; Figs. 5h, 7a, e), which may appear pore-filling, sometimes with euhedral crystal habit and often a pitted surface, titanium oxide (unbleached: avg. 0.1 %, bleached: avg. 0.1 %), replacive illite in alkali feldspars (unbleached: avg. 1 %, bleached: avg. 2 %; Figs. 5f, h) and accessory replacive kaolinite or chlorite that essentially do not vary between bleached and unbleached zones (Supplementary Table).

The arithmetic means of the main pore-filling authigenic cements quartz, illite and K-feldspar exceed the mean values of the unbleached zones by 3 to 6 %, while the mineral content of dolomite is too small to deduce a relationship (Fig. 7a). Similarly, for most of the nine samples quartz and illite cement contents are lower in unbleached zones (Figs. 7b, c, e), while the K-feldspar cement content is constantly higher in bleached zones (Fig. 7d). Authigenic minerals ac-

Fig. 5: Overview of mineral assemblage in bleached and un bleached zones. (**a**) Bleached zone with point and long contacts as well as minor iron oxide (FeOx) pigmented dust rims and with overall larger grain size (RB 28). (**b**) Unbleached zone with con cavo convex grain contacts, abundant deformed FeOx rich detritus, smaller grain sizes and less pore space (RB 28). (**c**) Intragranular macropore with remaining pigmented dust rim in bleached zone surrounded by pore filling illite (Ill pf, plain polarised light/ppl right, cross polarised light/xpl left). Also visible are authigenic quartz (Qtza) limited by euhedral K feldspar overgrowths (Fspa) on detrital grains (Qtz, Fsp, RB 17). (**d**) Close up of opaque and strongly deformed iron oxide grains and concavo convex contacts in an unbleached zone (RB 24). (**e**) Bleached zone with abundant pore filling cements and open pores in ppl (RB 28). (**f**) Same pore filling cements can be identified as K feldspar and quartz cements in xpl (Fspa, Qtza) with quartz growth stopping at euhedral K feld spar cements. Pore lining illite and illite replacing feldspars or rock fragments are observed (Ill pl, Ill rp, RB 28). (**g**) Unbleached zone with less K feldspar and syntaxial quartz cements (Fspa, Qtza), the latter stopping at the K feldspar overgrowth (RB 13). Abundant de formed FeOx grains are present (ppl right, xpl left). (**h**) Authi genic dolomite (Dol) growing in the pore space and on detrital grains as well as cement surfaces of quartz or K feldspar (Qtza, Fspa) and displaying a sometimes pitted appearance in ppl (left im age). Illite replaces detrital grains (RB 28, ppl left, xpl left).

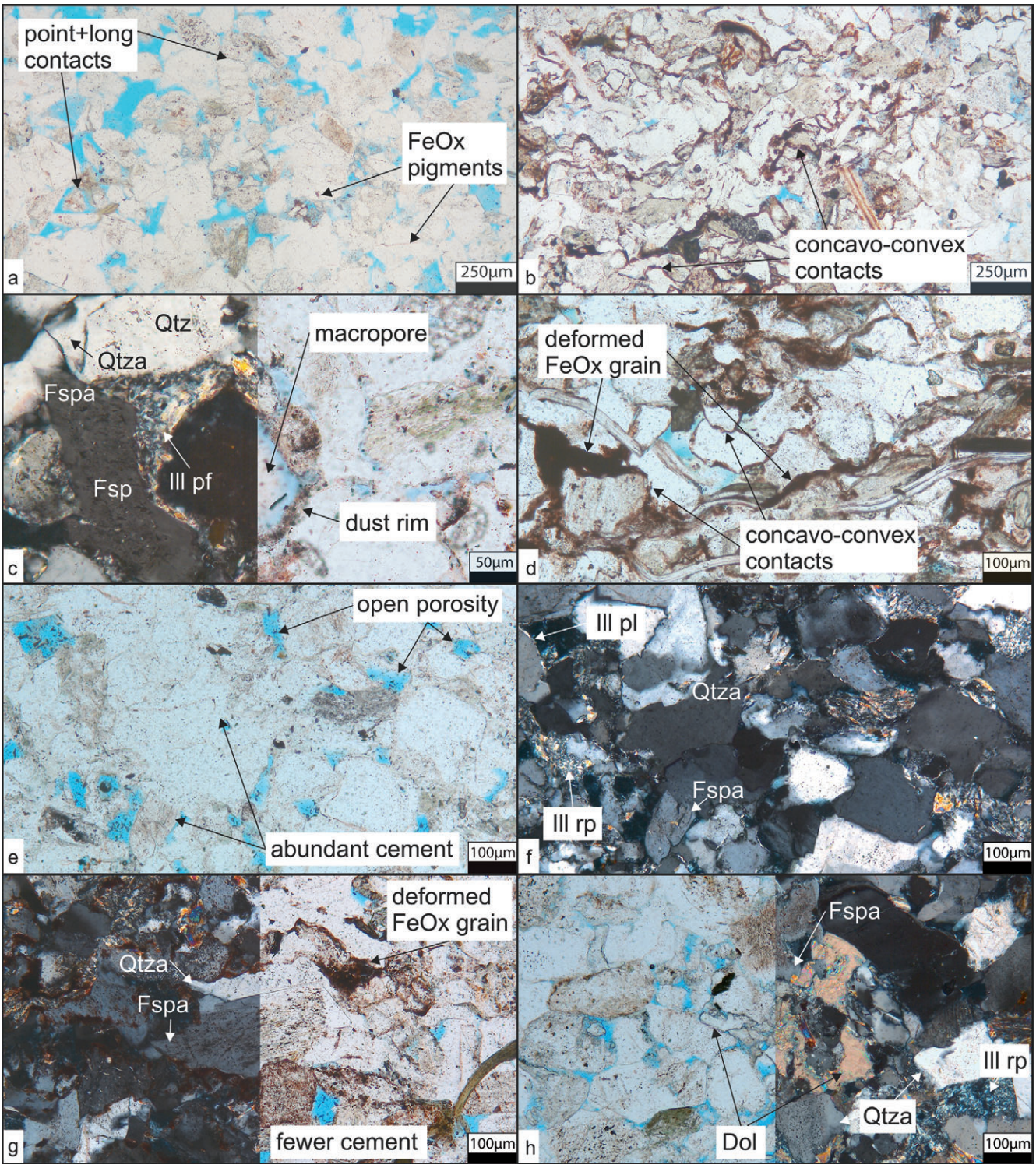
point+long contacts
FeOx pigments
a
250µm
concavo-convex contacts
b
250µm
Qtz
Qtza
Fspa
Fsp
Ill pf
macropore
dust rim
c
50µm
deformed FeOx grain
concavo-convex contacts
d
100µm
open porosity
abundant cement
e
100µm
Ill pl
Qtza
Fspa
Ill rp
f
100µm
Qtza
Fspa
deformed FeOx grain
fewer cement
g
100µm
Dol
Fspa
Ill rp
Qtza
h
100µm

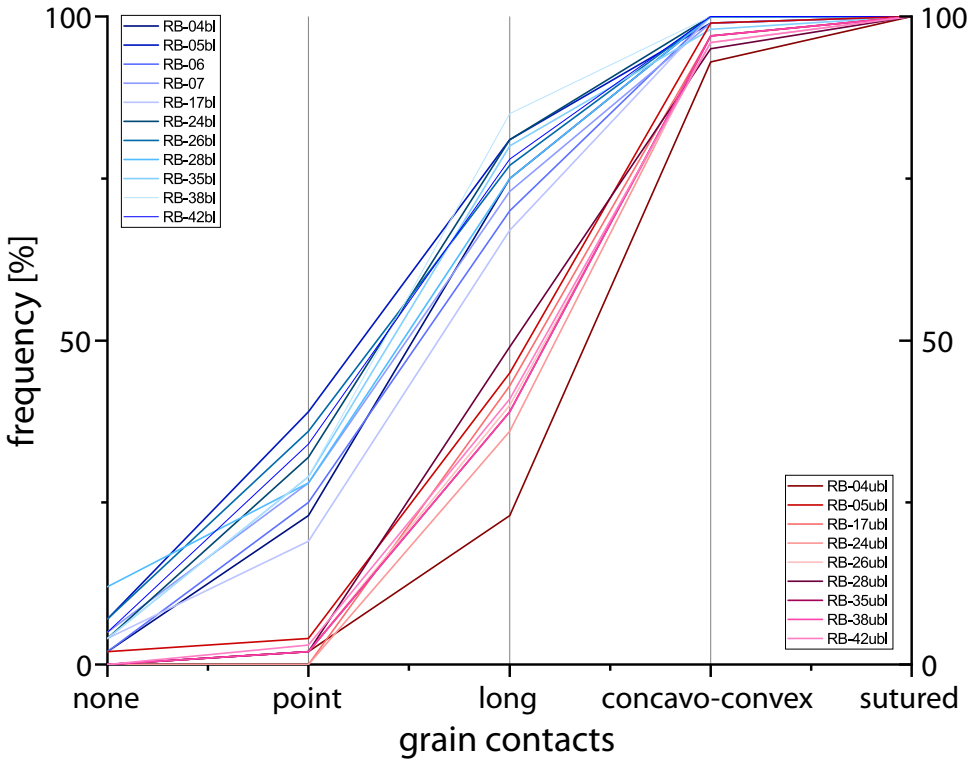

Fig. 6: Cumulative curve of measured grain contacts for unbleached (red) and bleached (blue) zones in all partially and fully bleached samples. The outline indicates the coherently different behaviour of unbleached and bleached zones with a much higher frequency of point contacts in bleached zones, contrasted by primarily concavo convex contacts in unbleached zones.

count for 23 % of the unbleached and for 34 % of the bleached zones.

Point counted porosities for unbleached zones range from 7 to 15 % (avg. 11 %), while bleached zones exhibit increased point counted porosities of 11 to 18 % (avg. 14 %; Fig. 8a). Values for all completely unbleached samples range from 9 % to 17 % (avg. 12 %; Fig. 8a). The trend towards higher porosities in bleached zones is also reflected by each sample (Fig. 8b). Pycnometer analyses show porosities of 11 to 19 % (avg. 16 %) (Schmidt et al. subm.). The average offset between petrophysical and point counted porosity accounts for ±3 % (Supplementary Table).

Compaction

The intergranular volume (IGV) of unbleached zones accounts for on average 27 % while bleached zones have an IGV of 39 % (Fig. 9). The average IGV value of 33 % of completely unbleached samples (max. 38 %, min. 25 %) matches the IGV of unbleached zones (max. 34 %, min. 14 %) and overlaps with lower values of bleached zones (max. 43 %, min. 27 %; Fig. 9). The outlier exhibiting the lowest IGV among the unbleached zones is a sample containing rip-up clasts (RB-17).

Considering compaction, unbleached zones show a compactional porosity loss (COPL) ranging from 17 to 36 % (avg. 25 %) and a cementational porosity loss (CEPL) ranging from 8 to 26 % (avg. 17 %; Fig. 10). In bleached zones the COPL values range from 3 to 24 % (avg. 9 %), while CEPL values range from 18 to 38 % (avg. 31 %; Fig. 10). The calculations after Lundegard (1992) suggest that almost all unbleached zones are dominated by compaction with the exception of two samples, whereas all bleached zones (except one sample) lose pore space primarily because of cementation (Fig. 10).

5. Discussion

5.1 Macroscopic description, texture and structure

Several studies present lamina-bound bleaching of red sandstones (Eichhubl et al. 2004; Nover et al. 2013; Pearce et al. 2011; Pudlo et al. 2012; Wendler et al. 2012). Discontinuous bleached spots of round to elliptical shape along a lamina indicate that bleaching is an authigenic process, likely unrelated to fluid flow, affecting an otherwise red deposit (Eichhubl et al. 2004). Stratigraphic constraints for bleaching (e.g. (Eichhubl et al. 2004) are not visible in the studied 10 m thick sandstone beds. Thus, bleaching can be described as occurring intraformational within the associated sandstone beds. All bleached zones show irregular and diffuse transi-

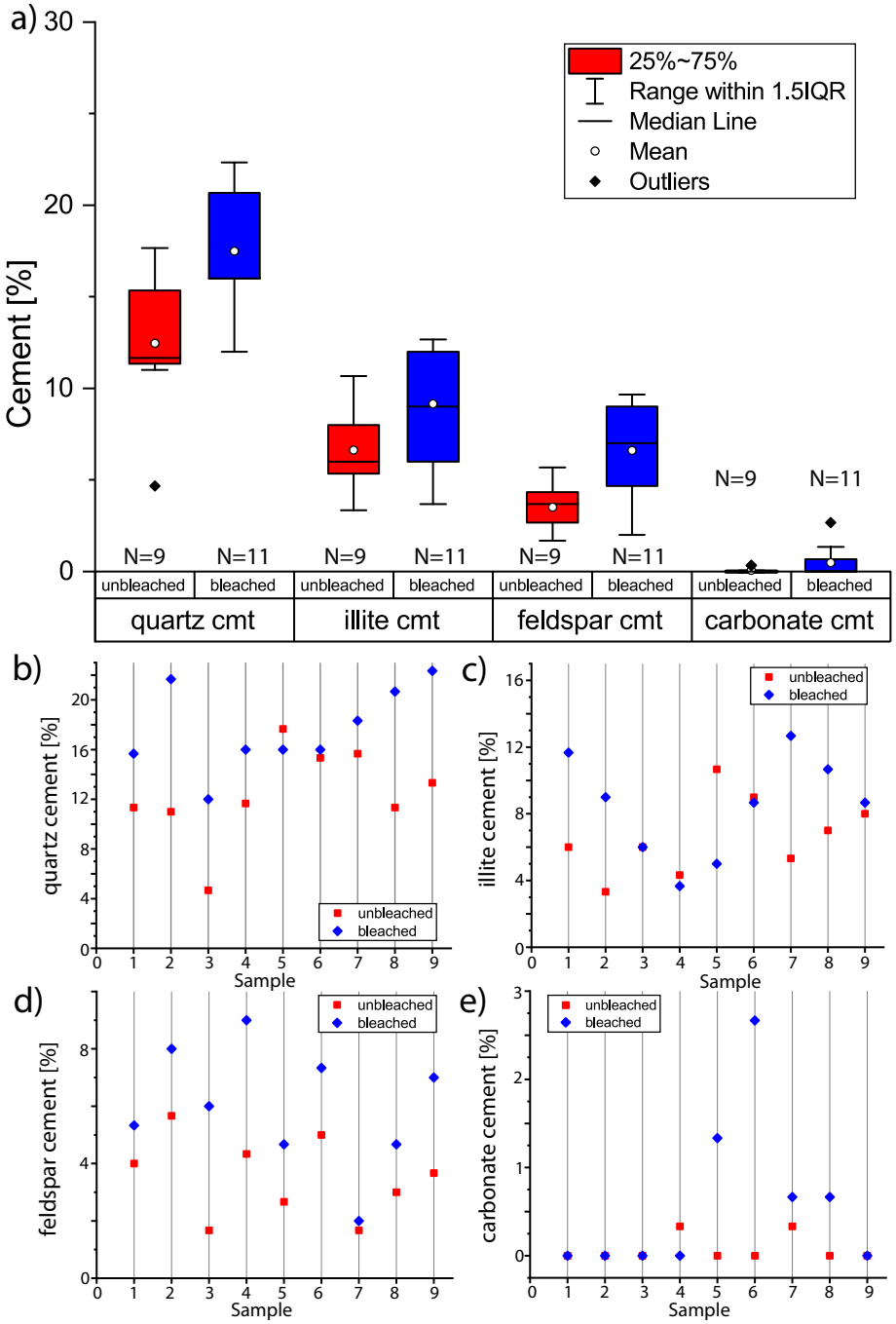

Fig. 7: (**a**) Box whisker plot of point counted cement contents (cmt) for all major authigenic phases. For quartz and K feldspar cements, the 50th percentile does not overlap and for all types of cement the mean volume in bleached zones exceeds that in the unbleached zones. For carbonate (dolomite) cement, no quantitative proof can be given with regard to average volumes of <1 %. (**b**) Scatter plot for quartz cement: The cement content of eight samples is higher where bleaching has taken place (outlier RB 35). (**c**) Scatter plot for illite cement: Cement occurrences are more frequent in bleached zones of five samples (outliers RB 24, RB 26, RB 28). (**d**) Scatter plot for feldspar ce ments: All samples contain more K feldspar cement in bleached zones. (**e**) Scatter plot for dolomite cements: No quantitative proof can be given for a preferential precipitation of dolomite cement with regard to small average volumes of <1 % and dolomite only being present in five of nine samples.

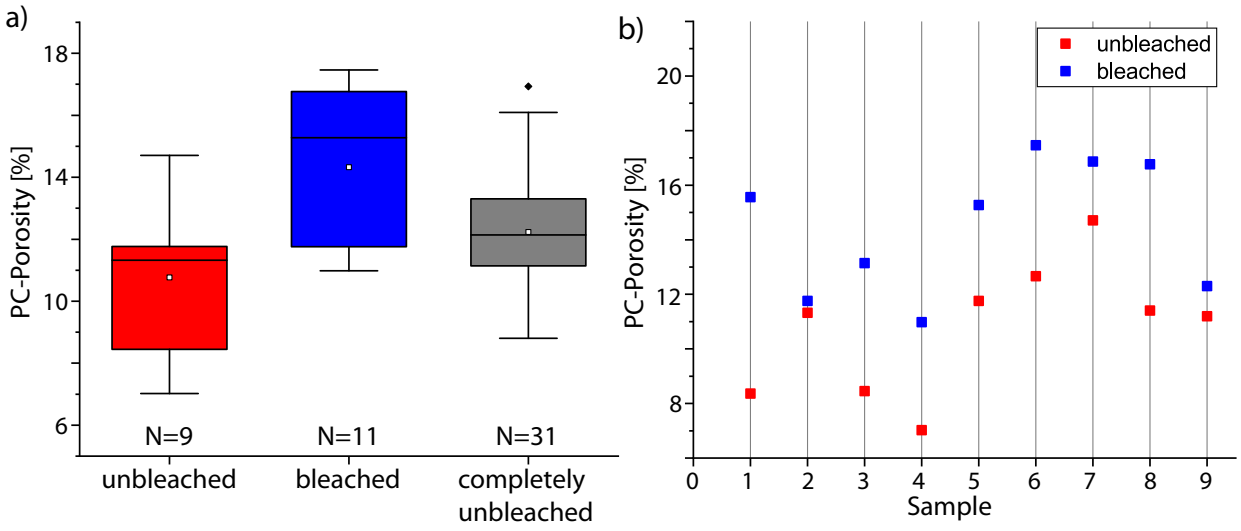

Fig. 8: (**a**) Box whisker plot of point count porosities (PC Porosity) plotted for the three types of material: unbleached zones (red), bleached zones (blue) and completely unbleached samples (grey). Bleached zones contain 3 % more pore space (avg. 14 %) than un bleached rock (avg. 11 %). Completely unbleached samples cover most of the porosity range of the unbleached zones in partially bleached samples but do not exceed the mean porosity of bleached zones. (**b**) The scatter plot for the nine partially bleached samples illustrates that bleaching in samples from the study area generally coincides with larger pore space.

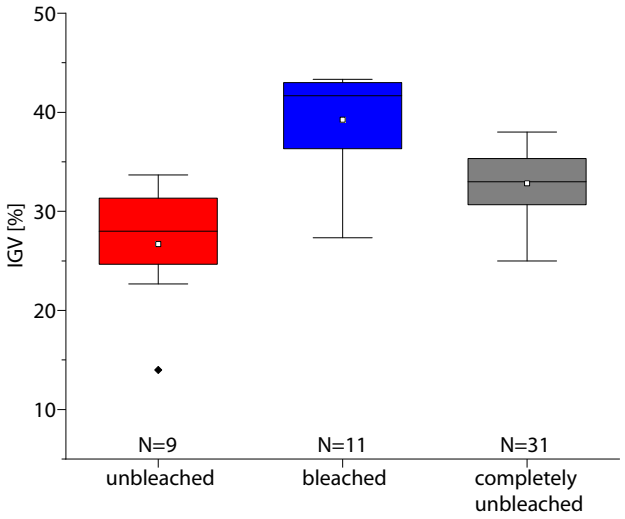

Fig. 9: Box whisker plot of the IGV plotted for the three types of samples: unbleached zones (red), bleached zones (blue) and com pletely unbleached samples (grey). Results for bleached and un bleached zones plot in distinctly different ranges. The completely unbleached samples have an average IGV of 33 % and match with the results of unbleached zones. The lower range of IGV values of bleached zones overlaps with the IGV of completely unbleached samples.

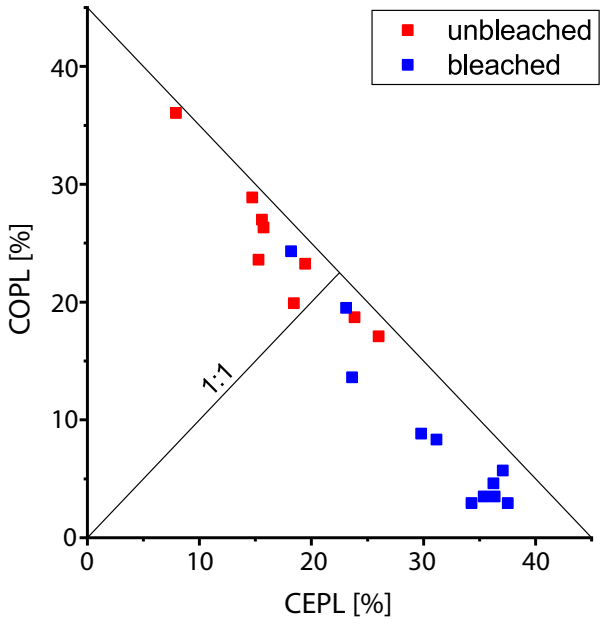

Fig. 10: Porosity loss by compaction and cementation for all sam ples. Compactional porosity loss (COPL) is plotted against cemen tational porosity loss (CEPL) after Lundegard (1992). Results from the unbleached zones plot mainly in the upper left triangle repre senting sample material that has lost porosity primarily due to com paction (seven of nine samples). Results from bleached zones mainly plot in the lower right triangle indicating a reduction in po rosity that is dominantly caused by cementation (ten of eleven sam ples).

tions across laminae (Figs. 2b, c). Additionally, pore-lining remnants of hematite dust rims, also underneath quartz or K-feldspar overgrowths (Figs. 5a, c), are present in bleached zones, which are known from the Lower and Middle Permian or Lower Triassic (Busch et al. 2017; Kunkel et al. 2018; Schöner & Gaupp 2005). Thus, bleaching removed hematite after its formation and after the associated reddening of the bulk rock (Walker 1975, 1967b).

Grain size analyses reveal that bleached zones contain larger grain sizes (avg. 173 µm) than the unbleached zones (avg. 146 µm). The latter matches well with the bulk sample analysis of the same study area with an average grain size of 148 µm. Although differences are relatively small (on average 27 µm; Fig. 3a) in the very fine- to fine-grained sandstones, this effect is shown for every partially bleached sample (Fig. 3b). This result is supported by other authors that have qualitatively noted more coarse-grained lithologies where bleaching took place (Chu et al. 2015; Eichhubl et al. 2004; Kunkel et al. 2018; Pudlo et al. 2012; Taylor & Barker 2002). Incorporating the thickness of a dust rim of 3 to 4 µm can also not explain the observed difference in grain diameters. Thus, grain size positively correlates with bleaching in the study area. Better sorting is also reported to facilitate bleaching (Beard & Weyl 1973; Pudlo et al. 2012) and may be supported by our data (Supplementary Table).

5.2 Petrography

5.2.1 Detrital composition in bleached and unbleached samples

The QFR-plot for bleached and unbleached zones in sandstones displays various rock compositions (Fig. 4, Supplementary Table). The average composition regarding quartz, feldspar and rock fragments varies insignificantly by at maximum 3 %. Equal amounts of quartz grains indicate a similar transport distance of the detritus and thus maturity of the unbleached and bleached zones. This also negates that bleached laminae are associated with depositional processes.

5.2.2 Authigenic composition in bleached and unbleached samples

All major cement phases like quartz, illite, feldspar and to a minor extent dolomite occur more frequently in bleached zones (Fig. 7). Similarly, other studies report more pronounced illitisation (Chu et al. 2015; Pudlo et al. 2012; Schöner & Gaupp 2005), more pronounced quartz cementation (Chu et al. 2015; Schöner & Gaupp 2005) as well as more iron-rich carbonate and chlorite cements in bleached rocks (Beyer 2015; Kunkel et al. 2018; Pudlo et al. 2012; Schöner & Gaupp 2005). Such observations are contradicted by some authors reporting major quartz cementation in unbleached Lower Triassic rocks (Reinecker et al. 2015).

The petrographic analyses (Figs. 5a, e, f) illustrate that abundant pore space in the bleached zones was available for higher quartz and K-feldspar cementation. In bleached zones compaction has a minor effect on the morphology of grain contacts with more than one quarter being point contacts and floating grains (24.2 % and 5.1 %, respectively) as opposed to 23.5 % of compaction-related concavo-convex and sutured contacts (Fig. 6). In unbleached zones more than half of the grain contacts are compaction-related with 56.9 % concavo-convex and 3.7 % sutured contacts. Hence, compaction in bleached zones must have been prevented by an early, framework stabilising cement phase in order to preserve uncompacted grain contacts and more pore space for quartz cementation during burial diagenesis. This is also supported by the higher calculated contact strength for bleached zones (Supplementary Table). The larger grain sizes may have, with higher permeabilities, facilitated more transport of available ions in the fluid for a more pronounced early diagenetic cementation along those laminae (Wilson et al. 2008).

A qualitative assessment yields that dolomite cements occur predominantly in the bleached laminae, which is not clearly visible from quantitative data (Fig. 7e). Fragmented, pore-filling dolomites have been linked to early diagenetic formation (Worden et al. 2018; Worden & Burley 2003), whereas sometimes euhedral, pore-filling dolomite growth on quartz and K-feldspar cement is considered to be a burial to uplift diagenetic process (Gaupp et al. 1993). The pitted appearance of the dolomite cement patches can be assigned to uplift diagenetic dissolution by meteoric waters (Fig. 5h; Worden et al. 2018). Staining did not reveal any significant iron content for the dolomites, nevertheless they could have incorporated minor amounts of iron after bleaching. To determine whether the iron left the system or was incorporated into the mineral assemblage, further analyses are needed as also chlorites replacing e.g. micas are only rarely observed (<1.3 %).

Based on petrographic observations some dolomite and euhedral K-feldspar cements predate quartz cements and predate mechanical compaction (Figs. 5c, g, h). Thus, they formed during early diagenesis and stabilised the grain framework (e.g. Gaupp & Okkerman 2011). Their stabilising effect inhibited compaction, preserving intergranular volume to be cemented by later pore-filling phases. As some iron oxide pigments are still recognisable in bleached zones underneath syntaxial quartz- and also K-feldspar cements as well as underneath some of the dolomite cement (Fig. 5a), it can be assumed that bleaching and thus the removal of most iron oxide phases took place during this period of feldspar cementation and mostly prior to syntaxial quartz cementation.

Intragranular macropores are restricted to bleached zones. Possible detrital grains, which might have been dissolved to form these intragranular macropores, are K-feldspar grains or rock fragments, which can be observed as sometimes illitised remnants or voids (Figs. 5c, f, h). Schöner & Gaupp (2005) have linked macropores to the dissolution of feldspars and lithoclasts, while Kunkel et al. (2018) also proposed the leaching of early cements, e.g. sulphate and carbonate as well as feldspar. Feldspar dissolution constitutes a source for potassium ions as well as relatively immo-

bile aluminum, allowing for a proximal precipitation of pore-filling illite (Bjørlykke 2014; Hayes & Boles 1992; Thyne et al. 2001). Feldspars thus constitute the most likely origin for macropores with illitisation (Figs. 5f, g).

Two types of burial diagenetic illite are more prominent in the bleached zones (Supplementary Table). Dense, primarily pore-filling illite is occasionally present around pigmented hematite dust rims surrounding intragranular macropores (Fig. 5c), while meshwork illite locally also fills intragranular macropores (Figs. 5f, h). In order to preserve intragranular macropores, they must have formed after mechanical compaction. Similarly, illitisation of feldspar grains, resulting in intragranular illite meshwork, likely postdates intragranular macropore formation and compaction (Molenaar & Felder 2018). This process added secondary intragranular porosity (Figs. 5f, h). Illite replacements are associated with temperatures of commonly above 100 °C and thus burial diagenesis (Bjørkum et al. 1993; Lander & Bonnell 2010; Morad et al. 2010) although precipitation may also start at lower temperatures (Bauer et al. 2000, 1998; Weibel 1999; Wilkinson et al. 2006; Ziegler 2006). Observations of a pronounced illitisation in bleached samples also correspond with other studies (Chu et al. 2015; Gaupp & Schöner 2008; Pudlo et al. 2012; Schöner & Gaupp 2005) and indicate a burial diagenetic timing for the bleaching process.

The petrographic assessment yields 3 % more porosity in bleached zones (Fig. 8a), which is consistent with several publications (Gaupp & Schöner 2008; Kunkel et al. 2018; Pudlo et al. 2012; Reinecker et al. 2015; Schöner & Gaupp 2005; Wendler et al. 2012) and also with observations in petrographic images (Figs. 5a, b). However, the contribution of dissolution and resulting intragranular macropores contributes with only 0.4 and 1.1 % to porosity in unbleached and bleached zones, respectively (Supplementary Table). Higher porosity and permeability are causally linked with larger grain size as was shown for different grain size classes like fine-grained and medium-grained (Bloch 1991; Chilingar 1964). For point counted porosities this correlation exists also at small-scale grain size changes as they occur between unbleached and bleached zones of this study (Fig. 3). Similarly, sorting is described to positively correlate with porosity and permeability (Beard & Weyl 1973), an effect that might also be present in this data set (Supplementary Table).

5.3 Compaction

Unbleached laminae are more compacted than bleached laminae, reflected by grain contacts and lower intergranular volume (avg. 27 %, max. 34 %, min. 14 %) than in bleached laminae (avg. 39 %, max. 43 %, min. 27 %). The grain contacts in unbleached areas (dominated by concavo-convex and sutured contacts with 56.9 % and 3.7 %, respectively) imply stronger pressure dissolution (chemical compaction) at grain contacts often covered by an illitic clay mineral. This reduction in intergranular volume results in smaller porosities and presumably permeabilities than in the bleached layers. The bleached layers contain more abundant K-feldspar and quartz cements reflected by 29.3 % point contacts and floating grains and almost no sutured contacts. All of which can potentially preserve higher intergranular volumes via framework stabilisation.

Values for porosity loss by compaction versus cementation are distinctly different for unbleached and bleached zones. The COPL-CEPL plot after Lundegard (1992) supports the optical assessment in that unbleached samples show a more pronounced compactional porosity loss than the bleached samples (Fig. 10). The presence of early syntaxial K-feldspar cements in the now-bleached areas preserved the intergranular volume and preserved porosity and now bleached permeability. The bleaching fluids then discoloured the more coarse-grained laminae with higher porosity/permeability and larger fluid volumes to sufficiently react with the surrounding minerals.

5.4 Deriving possible bleaching processes

Bleaching has been encountered in close paragenesis with bitumen stains and thus organic matter, forming diagenetic clay mineral phases and removing hematite in a variety of case studies (Beitler et al. 2003; Gaupp & Schöner 2008; Hilse et al. 2010; Pudlo et al. 2012; Schöner & Gaupp 2005). Kunkel et al. (2018) describe bleached lithologies as a special diagenesis type and link its formation to meteoric fluids. Other studies analysed stable carbon isotopy of calcites associated with bleaching and interpreted a volcanic or meteoric source (Kasch et al. 2010; Wendler et al. 2012). The absence of bitumen stains in samples from the study area and a lack of evidence for hydrocarbon-bearing underlying strata in the region suggests that no organic matter sourcing, e.g. organic acids or methane, was involved in partial bleaching of the red lithology (Beitler et al. 2003; Eichhubl et al. 2004; Gaupp & Schöner 2008; Okrusch et al. 2011). The absence of organic matter also affects bacterial and thermochemical sulphate reduction, which can be excluded as major bleaching mechanism (Machel 2001). The presence of volcanic dykes in the Spessart region may point toward a volcanic source of reducing fluids as it was proposed for Buntsandstein deposits in the Palatinate Forest (Baaske 1999; Peschel 2013). But as dykes are assigned to the Upper Cretaceous to Tertiary (Okrusch et al. 2011), they can hardly coincide with an early burial diagenetic bleaching process as it is proposed in this study (Fig. 11). Pedogenesis, also known to cause a colour alteration or colour mottling in Lower Triassic deposits, is ruled out as a cause, since characteristic features like rootlets, nodular carbonate cementation, or calcrete formation have not been encountered in the outcrop (Molenaar 1984; Ortlam 1974).

Reducing brines from underlying salt are considered equally unlikely as cause for the bleaching, because the study area is situated at the former Triassic basin margin and underlying evaporitic successions of the Upper Permian Zechstein Group are unknown (Okrusch et al. 2011). Furthermore, no pyrite neoformation was registered during point counting, which would have indicated bleaching by

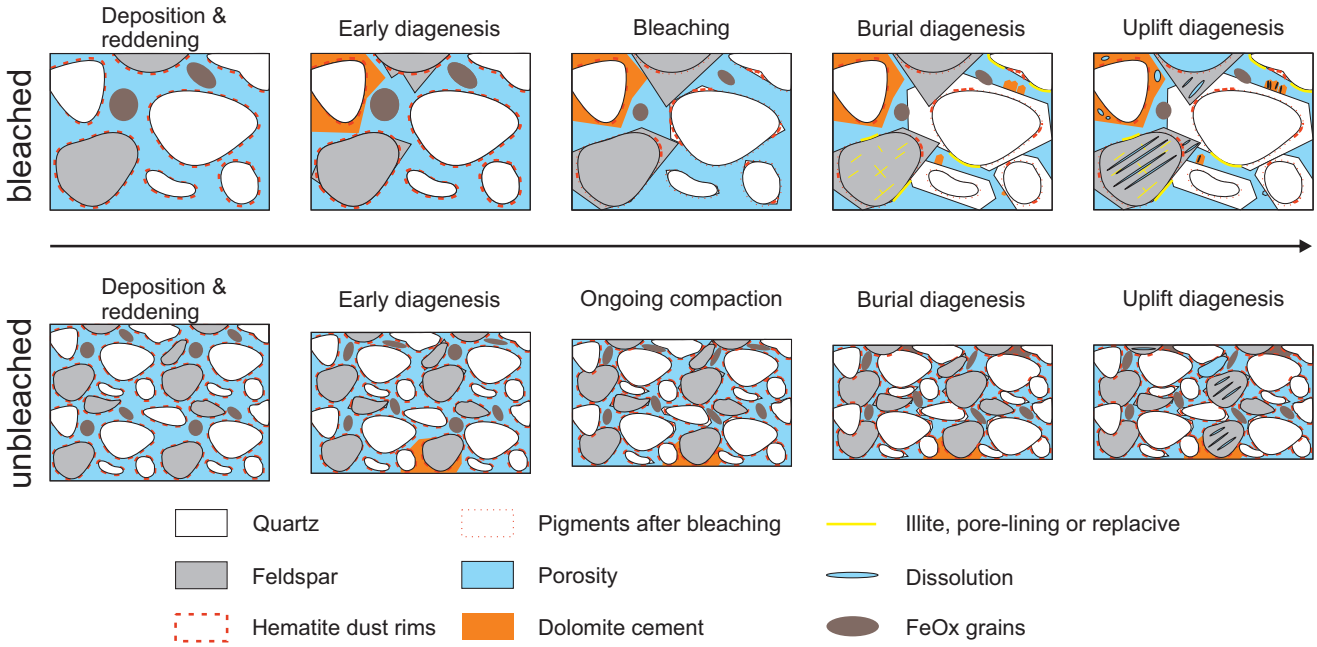

Fig. 11: Schematic overview of the bleaching process and diagenetic alterations. The upper row displays the temporal diagenetic alteration in the more coarse grained laminae with cementational porosity loss and carbonate and feldspar dissolution during uplift. The lower row shows the alteration in the finer grained unbleached laminae with compactional porosity loss, less pore space and more chemical compac tion on sutured and concavo convex grain contacts (lower row).

H_2S (Parry et al. 2004). However, reducing fluids from the overlying Muschelkalk sea with local evaporation pans (Okrusch et al. 2011) may have caused lamina-bound to pervasive bleaching in the sampled outcrop.

6. Conclusion

Bleached zones exhibit a grain size larger by 27 µm and to a minor extent better sorting. The present-day mineralogy is similar but porosities are on average 3 % higher in bleached laminae and thus reflect better reservoir quality. It can be assumed that initially better porosity and permeability enabled the fluid flow along specific laminae and their bleaching.

Compaction is higher in unbleached zones featuring primarily concavo-convex and sutured contacts (61 % vs. 24 % in bleached zones) and a lower IGV (27 % vs. 39 % in bleached zones).

Early diagenetic cement phases (dolomite and K-feldspar cement) stabilised the grain framework during compaction in bleached zones, preserving initially higher porosities and thus pathways that enabled bleaching. Bleached zones show a larger intergranular volume available to burial diagenetic quartz cementation, and exhibit 11 % more diagenetic minerals. Intragranular macropores are limited to bleached laminae and form secondary porosity. They are occasionally filled with illite fibres and formed post-compaction by the dissolution of feldspars and rock fragments. The more coarse-grained and more quartz- and feldspar-cemented bleached laminae exhibit higher IGV and point counted porosity. Those laminae also allowed subsequent leaching of detrital grains (rock fragments and feldspars) and minor amounts of carbonate cements during uplift diagenesis due to their likely higher initial permeability. In contrast, finer-grained laminae show more compaction reducing available intergranular volumes for cementation and reducing porosity and permeability and thus reservoir quality.

Overall, bleaching is promoted in laminae with larger initial grain size. Bleaching is thus the consequence and not the cause of primarily better permeability along single laminae.

7. Acknowledgements

We thank the Bamberger Natursteinwerke GmbH for granting access to their quarry and especially Paulus Sinner who provided a lot of support and information on-site. We thankfully acknowledge constructive comments by Heinz-Gerd Röhling, Reinhard Gaupp and Robert Lippmann.

8. References

Amelung, W., Blume, H. P., Fleige, H., Horn, R., Kandeler, E., Kögel Knabner, I., Kretzschmar, R., Stahr, K. & Wilke, B. M. (2018): Anorganische Komponenten der Böden Minerale und Gesteine. In: Blume, H. P., Brümmer, G.W., Horn, R., Kandeler, E., Kögel Knabner, I., Kretzschmar, R. & Stahr, K.: Scheffer/Schachtschabel: Lehrbuch der Bodenkunde: 11 62; Heidelberg (Springer); https://doi.org/10.1007/978 3 662 55871 3.

Baaske, U. (1999): Untersuchungen zur Diagenese des Buntsandsteins am Westrand des Rheingrabens (Region Bad Dürkheim/Neustadt a.d.W.). Diploma thesis Univ. Jena.

Bauer, A., Velde, B. & Berger, G. (1998): Kaolinite transformation in high molar KOH solutions. Appl. Geochem., 13: 619–629.

Bauer, A., Velde, B. & Gaupp, R. (2000): Experimental constraints on illite crystal morphology. Clay Miner., 35: 587–597.

Beard, D.C. & Weyl, P.K. (1973): Influence of texture on porosity and permeability of unconsolidated sand. AAPG Bull., 57: 349–369.

Becker, I., Wüstefeld, P., Koehrer, B., Felder, M. & Hilgers, C. (2017): Porosity and permeability variations in a tight gas sandstone reservoir analogue, Westphalian D, Lower Saxony Basin, NW Germany: Influence of depositional setting and diagenesis. J. Pet. Geol., 40: 363–389; https://doi.org/10.1111/jpg.12685.

Beitler, B., Chan, M.A. & Parry, W.T. (2003): Bleaching of Jurassic Navajo Sandstone on Colorado Plateau Laramide highs: Evidence of exhumed hydrocarbon supergiants? Geology, 31 (12): 1041–1044; https://doi.org/10.1130/G19794.1.

Beyer, D. (2015): Evolution of reservoir properties in the Lower Triassic aquifer sandstones of the Thuringian Syncline in Central Germany. Diss. Univ. Jena: 124 p.

Beyer, D., Kunkel, C., Hilse, U., Aehnelt, M., Pudlo, D., Voigt, T. & Gaupp, R. (2011): Reservoir properties and fluid circulation in Buntsandstein aquifer sandstones of the Thuringian Basin in Central Germany. In: Geophys. Res. Abstr., 13; EGU2011–13819; EGU General Assembly 2011, Vienna, Austria.

Beyer, D., Kunkel, C., Aehnelt, M., Pudlo, D., Voigt, T., Nover, G. & Gaupp, R. (2014): Influence of depositional environment and diagenesis on petrophysical properties of clastic sediments (Buntsandstein of the Thuringian Syncline, Central Germany). Z. Dt. Ges. Geowiss., 165 (3): 345–365; https://doi.org/10.1127/1860-1804/2014/0072.

Bjørkum, P.A., Walderhaug, O. & Aase, N.E. (1993): A model for the effect of illitization on porosity and quartz cementation of sandstones. J. Sediment. Petrol., 63: 1089–1091.

Bjørlykke, K. (2014): Relationships between depositional environments, burial history and rock properties. Some principal aspects of diagenetic process in sedimentary basins. Sediment. Geol., 301: 1–14.

Bloch, S. (1991): Empirical prediction of porosity and permeability in sandstones. AAPG Bull., 75: 1145–1160.

Burgess, D.T., Kettler, R.M. & Loope, D.B. (2016): The geologic context of wonderstone: A complex, outcrop scaled pattern of iron oxide cement. J. Sediment. Res., 86: 498–511; https://doi.org/10.2110/jsr.2016.35.

Busch, B., Hilgers, C., Gronen, L. & Adelmann, D. (2017): Cementation and structural diagenesis of fluvio aeolian Rotliegend sandstones, northern England. J. Geol. Soc. London, 174: 855–868; https://doi.org/10.1144/jgs2016-122.

Busch, B., Becker, I., Koehrer, B., Adelmann, D. & Hilgers, C. (2019): Porosity evolution of two Upper Carboniferous tight gas fluvial sandstone reservoirs: Impact of fractures and total cement volumes on reservoir quality. Mar. Pet. Geol., 100: 376–390; https://doi.org/10.1016/j.marpetgeo.2018.10.051.

Busch, B., Hilgers, C. & Adelmann, D. (2020): Reservoir quality controls on Rotliegend fluvio-aeolian wells in Germany and the Netherlands, Southern Permian Basin – Impact of grain coatings and cements. Mar. Pet. Geol., 112: 104075; https://doi.org/10.1016/j.marpetgeo.2019.104075.

Buurman, P. (1980): Palaeosols in the Reading Beds (Paleocene) of Alum Bay, Isle of Wight, U.K. Sedimentology, 27: 593–606.

Chan, M.A., Parry, W.T. & Bowman, J.R. (2000): Diagenetic hematite and manganese oxides and fault related fluid flow in Jurassic sandstones, Southeastern Utah. AAPG Bull., 84: 1281–1310.

Chilingar, G.V. (1964): Relationship between porosity, permeability and grain size distribution of sands and sandstones. Dev. Sedimentol., 1: 71–75.

Chu, H., Chi, G., Bosman, S. & Card, C. (2015): Diagenetic and geochemical studies of sandstones from drill core DV10-001 in the Athabasca basin, Canada, and implications for uranium mineralization. J. Geochem. Explor., 148: 206–230; https://doi.org/10.1016/j.gexplo.2014.10.002.

Deutsche Stratigraphische Kommission / German Stratigraphic Commission (ed.) (2002): Stratigraphische Tabelle von Deutschland 2002 / Stratigraphic Table of Germany 2002.

Dong, Y., Sanford, R.A., Locke, R.A., Cann, I.K., Mackie, R.I. & Fouke, B.W. (2014): Fe oxide grain coatings support bacterial Fe-reducing metabolisms in 1.7–2.0 km deep subsurface quartz arenite sandstone reservoirs of the Illinois Basin (USA). Front. Microbiol., 5; https://doi.org/10.3389/fmicb.2014.00511.

Eichhubl, P., Taylor, W.L., Pollard, D.D. & Aydin, A. (2004): Paleo-fluid flow and deformation in the Aztec Sandstone at the Valley of Fire, Nevada – Evidence for the coupling of hydrogeologic, diagenetic, and tectonic processes. Geol. Soc. Am., Bull., 116 (9/10): 1120–1136; https://doi.org/10.1130/B25446.1.

Folk, R.L. (1980): Petrology of sedimentary rocks: 184 p.; Austin, TX (Hemphill).

Folk, R.L. & Ward, W.C. (1957): Brazos river bar: A study in the significance of grain size parameters. J. Sediment. Petrol., 27: 3–26.

Freudenberger, W. (2016): Der Obere Buntsandstein in Kernbohrungen im südöstlichen Rhönvorland. In: Freudenberger, W., Friedlein, V., Schulze, M. & Specht, S. (ed.): Kernbohrungen in der Trias Unterfrankens. Geol. Bavarica, 114: 59–90.

Freudenberger, W., Geyer, G. & Schröder, B. (2013): Der Bunte Sandstein im nördlichen Bayern (nordwestliches Franken, Bruchschollenland und Randfazies im Untergrund). In: Deutsche Stratigraphische Kommission (Hg.; Koordination u. Redaktion: J. Lepper & H. G. Röhling für Subkommission Perm-Trias): Stratigraphie von Deutschland, XI: Buntsandstein. Schriftenr. Dt. Ges. Geowiss., 69: 547–582.

Füchtbauer, H. (1967): Der Einfluss des Ablagerungsmilieus auf die Sandsteindiagenese im Mittleren Buntsandstein. Sediment. Geol., 1: 159–179.

Füchtbauer, H. (1988): Sedimente und Sedimentgesteine; 4th ed.: 1141 p.; Stuttgart (Schweizerbart).

Garden, I.R., Guscott, S.C., Burley, S.D., Foxford, K.A., Walsh, J.J. & Marshall, J. (2001): An exhumed palaeo-hydrocarbon migration fairway in a faulted carrier system, Entrada Sandstone of SE Utah, USA. Geofluids, 1: 195–213.

Gaupp, R. & Okkerman, J.A. (2011): Diagenesis and reservoir quality of Rotliegend sandstones in the northern Netherlands – A review. In: Grötsch, J. & Gaupp, R. (ed.): The Permian Rotliegend of The Netherlands. Soc. Econ. Paleontol. Mineral., Spec. Publ., Spec. Publ., 98: 3–6; https://doi.org/10.2110/pec.11.98.

Gaupp, R. & Schöner, R. (2008): Intra reservoir generation of organic acids and late stage enhanced porosity in sandstones. AAPG Bull., Search and Discovery Article #40373.

Gaupp, R., Matter, A., Platt, J., Ramseyer, K. & Walzebuck, J. (1993): Diagenesis and fluid evolution of deeply buried Permian (Rotliegende) gas reservoirs, Northwest Germany. AAPG Bull., 77: 1111–1128.

Geyer, G. (2002): Geologie von Unterfranken und angrenzenden Regionen: 588 p.; Gotha (Klett Perthes).

Hagdorn, H., Nitsch, E., Aigner, T. & Simon, T. (2009): Field guide. In: International Triassic Field Workshop, Triassic of South west Germany, September 7 11, 2009, Tübingen and Ingelfin gen: 72 p.; http://www.stratigraphie.de/perm trias/trias work shops.html.

Haszeldine, R.S., Quinn, O., England, G., Wilkinson, M., Shipton, Z.K., Evans, J.P., Heath, J., Crossey, L., Ballentine, C.J. & Gra ham, C.M. (2005): Natural geochemical analogues for carbon dioxide storage in deep geological porous reservoirs, a United Kingdom perspective. Oil & Gas Sci. Technol., 60: 33 49; https://doi.org/10.2516/ogst:2005004.

Hayes, M.J. & Boles, J.R. (1992) : Volumetric relations between dissolved plagioclase and kaolinite in sandstones: Implications for aluminum mass transfer in the San Joaquin Basin, Califor nia. In: Houseknecht, D.W. & Pittman, E.D. (ed.): Origin, diagenesis, and petrophysics of clay minerals in sandstone. SEPM, Spec. Publ., 47: 111 123.

Hilse, U., Goepel, A., Pudlo, D., Heide, K. & Gaupp, R. (2010): Characterization of CO_2 induced (?) bleaching phenomena in German red bed sediments by combined geochemical and evolved gas analysis. In: EGU General Assembly 2010 Vienna/ Austria, 02.05 07.05.2010. Geophys. Res. Abstr., 12: 1 p.

Hurst, A. & Nadeau, P.H. (1995): Clay microporosity in reservoir sandstones: An application of quantitative electron microscopy in petrophysical evaluation. AAPG Bull., 79: 563 573.

Kasch, N., Kley, J., Köster, J. & Wendler, J. (2010): Fracture re lated fluid migration and fluid rock interaction in outcrop ana logues of Buntsandstein reservoir rocks (southern Thuringia and northern Hesse). In: EGU General Assembly 2010 Vi enna/Austria, 02.05 07.05.2010. Geophys. Res. Abstr., 12: 13194.

Kirkland, D.W., Denison, R.E. & Rooney, M.A. (1995): Diagenetic alteration of Permian strata at oil fields of south central Okla homa, USA. Mar. Pet. Geol., 12: 629 644.

Kunkel, C., Aehnelt, M., Pudlo, D., Kukowski, N., Totsche, K.U. & Gaupp, R. (2018): Subsurface aquifer heterogeneities of Lower Triassic clastic sediments in central Germany. Mar. Pet. Geol., 97: 209 222.

Lander, R.H. & Bonnell, L.M. (2010): A model for fibrous illite nucleation and growth in sandstones. AAPG Bull., 94 (8): 1161 1187; https://doi.org/10.1306/04211009121.

Lovley, D.R., Roden, E.E., Philips, E.J.P. & Woodward, J.C. (1993): Enzymatic iron and uranium reduction by sulfate reducing bac teria. Mar. Geol., 113: 41 53.

Lundegard, P.D. (1992): Sandstone porosity loss A “big picture” view of the importance of compaction. J. Sediment. Petrol., 62: 250 260.

Machel, H.G. (2001): Bacterial and thermochemical sulfate reduc tion in diagenetic settings Old and new insights. Sediment. Geol., 140: 143 175.

Mader, D. & Teyssen, T. (1985): Palaeoenvironmental interpreta tion of fluvial red beds by statistical analysis of paleocurrent data: Examples from the Buntsandstein (Lower Triassic) of the Eifel and Bavaria in the German Basin (Middle Europe). Sed iment. Geol., 41: 1 74.

Makowitz, A. & Sibley, D. (2001): Crystal growth mechanisms of quartz overgrowths in a Cambrian quartz arenite. J. Sediment. Res., 71: 809 816.

Menning, M. (2018): Die Stratigraphische Tabelle von Deutschland 2016 (STD 2016) / The Stratigraphic Table of Germany 2016 (STG 2016). Z. Dt. Ges. Geowiss., 169 (2): 105 128.

Meschede, M. & Warr, L.N. (2019): The geology of Germany A process oriented approach. Regional Geology Reviews: 304 p.; Heidelberg (Springer).

Molenaar, N. (1984): Palaeopedogenic features and their palaeocli matological significance for the Nevremont Formation (Lower Givetian), the Northern Ardennes, Belgium. Palaeogeogr., Palaeoclimatol., Palaeoecol., 46: 325 344.

Molenaar, N. & Felder, M. (2018): Clay cutans and the origin of illite rim cement: An example from the siliciclastic Rotliegend sandstone in the Dutch Southern Permian Basin. J. Sediment. Res., 88: 641 658; https://doi.org/10.2110/jsr.2018.33.

Morad, S., Al Ramadan, K., Ketzer, J.M. & De Ros, L.F. (2010): The impact of diagenesis on the heterogeneity of sandstone res ervoirs: A review of the role of depositional facies and sequence stratigraphy. AAPG Bull., 94: 1267 1309; https://doi.org/ 10.1306/04211009178.

Nover, G., Von Der Gönna, J., Heikamp, S. & Köster, J. (2013): Changes of petrophysical properties of sandstones due to inter action with supercritical carbon dioxide A laboratory study. Eur. J. Mineral., 25 (3): 317 329; https://doi.org/10.1127/0935 1221/2013/0025 2295.

Okrusch, M., Geyer, G. & Lorenz, J. (2011): Spessart Geologi sche Entwicklung und Struktur, Gesteine und Minerale. Sammlung geologischer Führer, 106: 398 p.; Stuttgart (Born traeger).

Ortlam, D. (1974): Inhalt und Bedeutung fossiler Bodenkomplexe in Perm und Trias von Mitteleuropa. Geol. Rundsch., 63: 850 884.

Parry, W.T., Chan, M.A. & Beitler, B. (2004): Chemical bleaching indicates episodes of fluid flow in deformation bands in sand stone. AAPG Bull., 88: 175 191.

Paxton, S.T., Szabo, J.O., Ajdukiewicz, J.M. & Klimentidis, R.E. (2002): Construction of an intergranular volume compaction curve for evaluating and predicting compaction and porosity loss in rigid grain sandstone reservoirs. AAPG Bull., 86: 2047 2067.

Pearce, J.M., Kirby, G.A., Lacinska, A., Bateson, L., Wagner, D., Rochelle, C.A. & Cassidy, M. (2011): Reservoir scale CO_2 fluid rock interactions: Preliminary results from field investiga tions in the Paradox Basin, Southeast Utah. Energy Procedia, 4: 5058 5065; https://doi.org/10.1016/j.egypro.2011.02.479.

Peschel, S.E. (2013): Der Einfluss des Forster Vulkanismus auf die Diagenese des gebleichten Buntsandsteins des Pfälzer Waldes parallel zum Rheingrabenrand. Diploma thesis Univ. Jena.

Pudlo, D., Reitenbach, V., Albrecht, D., Ganzer, L., Gernert, U., Wienand, J., Kohlhepp, B. & Gaupp, R. (2012): The impact of diagenetic fluid rock reactions on Rotliegend sandstone com position and petrophysical properties (Altmark area, central Germany). Environ. Earth Sci., 67: 369 384; https://doi.org/ 10.1007/s12665 012 1723 y.

Reinecker, J., Grobe, R., Hochschild, T., Bauer, J., Meier, S., Phil ipp, S., Filomena, M., Stollhofen, H., Bechstädt, T., Drews, T., Miernik, G., Soyk, D. & Melchert, B. (2015): Verbundprojekt AuGE: Aufschlussanalogstudien und ihre Anwendbarkeit in der geothermischen Exploration Entwicklung von Methoden zur Ermittlung von Permeabilitäten und Transmissivitäten aus Reservoir Informationen des Oberrheingrabens Outcrop ana logue studies in geothermal exploration. Schlussbericht Teil projekt A: 75 p.; Karlsruhe (GeoThermal Engineering GmbH).

Röhling, H. G. & Lepper, J. (2013): Paläogeographie des Mittel europäischen Beckens während der tieferen Trias (Buntsand stein). In: Deutsche Stratigraphische Kommission (Hg.; Ko ordination u. Redaktion: J. Lepper & H. G. Röhling für Sub

kommission Perm Trias): Stratigraphie von Deutschland, XI: Buntsandstein. Schriftenr. Dt. Ges. Geowiss, 69: 43 67.

Röhling, H. G., Lepper, J., Diehl, M., Dittrich, D., Freudenberger, W., Friedlein, V., Hug Diegel, N. & Nitsch, E. (2018): Der Buntsandstein in der Stratigraphischen Tabelle von Deutsch land 2016 / The Buntsandstein Group in the Stratigraphic Table of Germany 2016. Z. Dt. Ges. Geowiss., 169 (2): 151 180; https://doi.org/10.1127/zdgg/2018/0132.

Schmidt, C., Busch, B. & Hilgers, C. (subm.): Lateral variations of detrital, authigenic, and petrophysical properties in lower Trias sic fluvial sandstones. Z. Dt. Ges. Geowiss. (submitted).

Schöner, R. & Gaupp, R. (2005): Contrasting red bed diagenesis: The southern and northern margin of the Central European Ba sin. Int. J. Earth Sci., 94: 897 916; https://doi.org/10.1007/ s00531 005 0004 3.

Schumacher, D. (1996): Hydrocarbon induced alteration of soils and sediments. In: Schumacher, D. & Abrams, M.A. (ed.): Hydrocarbon migration and its near surface expression. AAPG Mem., 66: 71 89.

Shebl, M.A. & Surdam, R.C. (1996): Redox reactions in hydrocar bon clastic reservoirs: Experimental validation of this mecha nism for porosity enhancement. Chem. Geol., 132: 103 117.

Taylor, J.M. (1950): Pore space reduction in sandstones. AAPG Bull., 34: 701 716.

Taylor, S. & Barker, R. (2002): Resistivity of partially saturated Triassic Sandstone. Geophys. Prospect., 50: 603 613.

Thyne, G., Boudreau, B.P., Ramm, M. & Midtbø, R.E. (2001): Sim ulation of potassium feldspar dissolution and illitization in the Statfjord Formation, North Sea. AAPG Bull., 85: 621 635.

Udden, J.A. (1914): Mechanical composition of clastic sediments. Geol. Soc. Am., Bull., 25: 655 744.

Walderhaug, O. (2000): Modeling quartz cementation and porosity in Middle Jurassic Brent Group sandstones of the Kvitebjørn Field, Northern North Sea. AAPG Bull., 84: 1325 1339.

Walderhaug, O., Eliassen, A. & Aase, N.E. (2012): Prediction of permeability in quartz rich sandstones: Examples from the Norwegian continental shelf and the Fontainebleau Sandstone. J. Sediment. Res., 82: 899 912; https://doi.org/10.2110/jsr. 2012.79.

Walker, T.R. (1967a): Formation of red beds in modern and ancient deserts. Geol. Soc. Am., Bull., 78: 353 368.

Walker, T.R. (1967b): Color of recent sediments in tropical Mexico: A contribution to the origin of red beds. Geol. Soc. Am., Bull., 78: 917 920.

Walker, T.R. (1975): Red beds in the western interior of the United States. In: McKee, E.D., Crosby, E.J. et al.: Paleotectonic in vestigations of the Pennsylvanian System in the United States. U.S. Geol. Surv., Prof. Pap., 853: 49 56.

Walker, T.R., Waugh, B. & Grone, A.J. (1978): Diagenesis in first cycle desert alluvium of Cenozoic age, southwestern United States and northwestern Mexico. Geol. Soc. Am., Bull., 89: 19 32.

Weibel, R. (1998): Diagenesis in oxidising and locally reducing conditions An example from the Triassic Skagerrak Forma tion, Denmark. Sediment. Geol., 121: 259 276.

Weibel, R. (1999): Effects of burial on the clay assemblages in the Triassic Skagerrak Formation, Denmark. Clay Miner., 34: 619 635.

Wendler, J., Köster, J., Götze, J., Kasch, N., Zisser, N., Kley, J., Pudlo, D., Nover, G. & Gaupp, R. (2012): Carbonate diagenesis and feldspar alteration in fracture related bleaching zones (Buntsandstein, central Germany): Possible link to CO_2 influ enced fluid mineral reactions. Int. J. Earth Sci., 101: 159 176; https://doi.org/10.1007/s00531 011 0671 1.

Wentworth, C.K. (1922): A scale of grade and class terms for clastic sediments. J. Geol., 30: 377 392.

Wilkinson, M., Haszeldine, R.S. & Fallick, A.E. (2006): Jurassic and Cretaceous clays of the northern and central North Sea hy drocarbon reservoirs reviewed. Clay Miner., 41: 151 186; https://doi.org/10.1180/0009855064110197.

Wilson, A.M., Huettel, M. & Klein, S. (2008): Grain size and depo sitional environment as predictors of permeability in coastal marine sands. Estuar. Coast. Shelf Sci., 80 (1): 193 199; https://doi.org/10.1016/j.ecss.2008.06.011.

Wilson, J.C. & McBride, E.F. (1988): Compaction and porosity evolution of Pliocene sandstones, Ventura Basin, California. AAPG Bull., 72: 664 681.

Worden, R.H. & Burley, S.D. (2003): Sandstone diagenesis: The evolution of sand to stone. In: Burley, S.D. & Worden, R.H. (ed.): Sandstone diagenesis: Recent and ancient. Int. Assoc. Sedimentol., Reprint Ser., 4: 3 44.

Worden, R.H., Armitage, P.J. & Butcher, A.R. (2018): Petroleum reservoir quality prediction: Overview and contrasting ap proaches from sandstone and carbonate communities. In: Churchill, J.M., Csoma, A.E., Hollis, C., Lander, R.H. & Omma, J.E. (ed.): Reservoir quality of clastic and carbonate rocks: Analysis, modelling and prediction. Geol. Soc. Lon don, Spec. Publ., 435: 1 31.

Wüstefeld, P., Hilse, U., Koehrer, B., Adelmann, D. & Hilgers, C. (2017): Critical evaluation of an Upper Carboniferous tight gas sandstone reservoir analog: Diagenesis and petrophysical as pects. Mar. Pet. Geol., 86: 89 710; https://doi.org/10.1016/j. marpetgeo.2017.05.034.

Ziegler, K. (2006): Clay minerals of the Permian Rotliegend group in the North Sea and adjacent areas. Clay Miner., 41: 355 393; https://doi.org/10.1180/0009855064110200.

Ziegler, P.A. (1982): Triassic rifts and facies patterns in Western and Central Europe. Geol. Rundsch., 71: 747 772; https://doi. org/10.1007/BF01821101.

Ziegler, P.A. (1990): Geological atlas of Western and Central Eu rope; The Hague (Shell Int. Petroleum Mij.).

Electronic supplement

Supplementary material associated with this article is embedded in the pdf of this article. The online version of *Zeitschrift der Deutschen Gesellschaft für Geowissenschaften –Journal of Applied and Regional Geology* (*ZdGG*) is hosted at the journal's website www.schweizerbart.com/journals/zdgg. The publisher does not bear any liability for the lack of usability or correctness of supplementary material.

Supplementary Table: All petrographic and petrophysical data as well as calculated parameters for the state of compaction.

Please save the electronic supplement contained in this pdf-file by clicking the blue frame above. After saving rename the file extension to .zip (for security reasons Adobe does not allow to embed .exe, .zip, .rar etc. files).